Journal of Molecular Structure 1183 (2019) 256–262

Contents lists available at ScienceDirect

Journal of Molecular Structure

journal homepage: http://www.elsevier.com/locate/molstruc

A stable 1D mixed-valence CuI/CuII coordination polymer with photocatalytic reduction activity toward Cr(VI)

Jun Zhong, Xiao-Hong Yi, Peng Wang, Chong-Chen Wang*

Beijing Key Laboratory of Functional Materials for Building Structure and Environment Remediation/Beijing Advanced Innovation Center for Future Urban Design, Beijing University of Civil Engineering and Architecture, Beijing, 100044, China

ARTICLE INFO

Article history:
Received 5 December 2018
Received in revised form
13 January 2019
Accepted 29 January 2019
Available online 1 February 2019

Keywords:
Coordination polymer
Hexavalent chromium
Photocatalysis
Copper
Mixed-valence

ABSTRACT

A new one-dimensional coordination polymer, **$[Cu^{II}(L)_2][Cu^{I}(bpy)]_2\cdot 4H_2O$ (BUC-20)** (H_2L = *cis*-1,3-dibenzyl-2-imidazolidone-4,5-dicarboxylic acid, bpy = 4,4-bipyridine), was synthesized solvothermal condition. The crystal structure of **BUC-20** was analyzed, and its properties like band energy, water stability, and photocurrent were clarified. **BUC-20** exhibited outstanding photocatalytic Cr(VI) performance upon the UV light irradiation under acid condition, which was superior to those of existing photocatalysts. The photocatalytic performance was not influenced by the presence of inorganic ions, which was affirmed by the introduction real surface water to prepare simulated wastewater. **BUC-20** exhibited good water stability, and could be used several runs without significant efficiency decrease.

1. Introduction

Chromium compounds like Cr(VI) are widely used in electroplating, stainless steel production, leather tanning, textile manufacturing, and even wood preservation [1,2]. The presence of Cr(VI) at ppb level in aquatic system and drinking water source can result into severe threat to creature. It was essential to remediate Cr(VI) in environment via toxicity reduction, removal technologies and containment technologies. The photocatalytic transformation from highly toxic Cr(VI) into lowly toxic Cr(III) is preferred due to that Cr(III) can be easily precipitated into $Cr(OH)_3$ at higher pH [2]. To enhance the photocatalytic performance toward Cr(VI) reduction, it was a top priority to find efficient photocatalysts.

Just recently, coordination polymers (CPs) including metal-organic frameworks (MOFs) attracted increasing attentions due to their fascinating structure [3–8] along with their versatile properties and potential applications like gas separation [9–12], gas storage [13–16], catalysis [17–20], fluorescence [21–23], pollutants adsorption [24–32], photocatalysis [2,33–37] and so on. The design and synthesis of mixed-valent Cu^{I}/Cu^{II} coordination polymers (including MOFs) has paid great attentions because of their instinct electronic, luminescent and biological properties [38–41]. Especially, MOFs were used as photocatalysts to conduct photocatalytic reactions due to the synergistic effect of their metal or metal-oxygen clusters and organic linkers [2,33]. To design and synthesize more excellent MOFs photocatalysts with high water/chemical/photo stability triggered significant enthusiasm in MOFs field. It was deemed that 1D or 2D coordination polymers (or MOFs) can exhibit higher photocatalytic performance than 3D MOFs due to their electrical conductivity [2,33,42,43].

Some 2D CPs like **BUC-21**, **BUC-66** and **BUC-67** were constructed from *cis*-1,3-dibenzyl-2-imidazolidone-4,5-dicarboxylic acid (H_2L) and Zn/Cd/Co salts with the aid of secondary organic linkers like 4,4′-bipyridine (bpy), which displayed outstanding Cr(VI) reduction via photocatalysis under UV light irradiation [34,44]. Especially, g-C_3N_4 was introduced to fabricate g-C_3N_4/BUC-21 heterojunction to achieve enhanced Cr(VI) reduction under simulated sunlight or even real sunlight [44]. In this study, H_2L and bpy (as illustrated in Scheme 1) were selected to build a new infinite one-dimensional (1D) coordination polymer **$[Cu^{II}(L)_2][Cu^{I}(bpy)]_2\cdot 4H_2O$ (BUC-20)** under solvothermal condition, which exhibited superior photocatalytic Cr(VI) reduction under UV light illumination.

2. Experimental

2.1. Materials and characterizations

All commercially available chemicals are reagent grade, and

* Corresponding author.
E-mail address: wangchongchen@bucea.edu.cn (C.-C. Wang).

https://doi.org/10.1016/j.molstruc.2019.01.097
0022-2860/

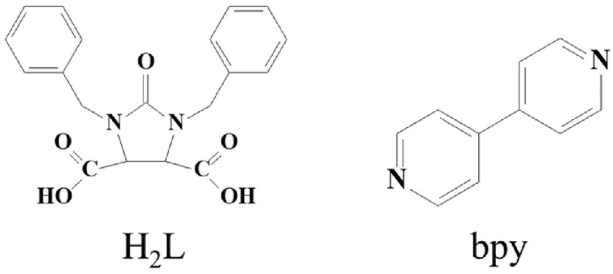

Scheme 1. Structural formulae of H_2L and bpy.

used as received without further treatment. Fourier transform infrared spectra (FTIR) were recorded on a Nicolet 6700 FTIR spectrometer with KBr pellets in the region from 4000 cm^{-1} to 400 cm^{-1}. Powder X-ray diffraction (XRD) patterns were recorded on DX-2700B X-ray diffractometer with Cu Kα radiation in the 2θ range of 5–50°. The zeta potentials of sample under different pH were determined by a JS94H zeta potential analyzer at a room temperature of 25 °C. UV–vis diffuse reflectance spectra (DRS) were measured by a PerkinElmer Lambda 650S UV–vis spectrophotometer in the range of 200–800 nm with $BaSO_4$ as a 100% reflectance standard. Thermal gravimetric analysis (TGA) was conducted from room temperature to 800 °C at a flow rate of 10 °C min^{-1} in an air stream on a DTU-3c instrument using α-Al_2O_3 as reference.

2.2. Synthesis of $[Cu^{II}(L)_2][Cu^{I}(bpy)]_2{\cdot}4H_2O$ (BUC-20)

A mixture of H_2L (0.3 mmol, 106.3 mg), bpy (0.3 mmol, 46.9 mg), $Cu(NO_3)_2{\cdot}2.5H_2O$ (0.3 mmol, 139.5 mg), ethanol (5 mL) and deionized water (10 mL) was transferred into Teflon-lined stainless steel Parr bomb, and was heated at 140 °C for 72 h. Green square crystals of **$[Cu^{II}(L)_2][Cu^{I}(bpy)]_2{\cdot}4H_2O$** (**BUC-20**, yield 86% based on $Cu(NO_3)_2{\cdot}2.5H_2O$), were collected by isolating and wishing with deionized water and ethanol in turn, after cooling down slowly to room temperature. *Anal. Calc.* for **BUC-20** ($C_{58}H_{56}Cu_3N_8O_{14}$): C, 54.4%; N, 8.8%; H, 4.4%. Found: C, 54.5%; N, 8.8%; H, 4.5%. FTIR (KBr)/cm^{-1}: 3434, 1629, 1612, 1533, 1493, 1447, 1420, 1306, 1225, 1074, 860, 819, 771, 732, 699, 669, 642, 568, 489, 430.

2.3. X-ray crystallography

X-ray single-crystal data of **BUC-20** was obtained with a Bruker CCD X-ray diffractometer using Graphite furnace monochromatized Mo Kα radiation ($\lambda = 0.71073$ Å) by the φ-ω mode at 298 (2) K. single-crystal data of **BUC-20** was collected and extracted using SMART [45] and SANT [46] software respectively, and modification of experience absorption was performed by the SADABS program [47]. Finally, the structure of **BUC-20** was refined based on the full-matrix-least squares techniques on F^2 with anisotropic thermal parameters for all non-hydrogen atoms. All hydrogen atoms were allowed to ride on their respective parent atoms. All structural calculations were carried out using the SHELX-97 program package [48]. Crystallographic data and structural refinement for **BUC-20** were summarized in Table 1.

2.4. Electrochemistry determination

The working electrodes preparation: 5.0 mg **BUC-20** powder samples (with the particle sizes less than 0.074 mm) were mixed with 400.0 μL ethanol/Nafion ($v/v = 19/1$) matrix, which was dispersed under sonication for 30 min. 10.0 μL prepared slurry was drop-casted onto the surface of a FTO substrate (1.0 cm × 1.0 cm), and then dried in air at 353 K for 30 min. This step was repeated five times to ensure the uniform coverage of **BUC-20** samples on the FTO substrate.

The electrochemical measurements were performed on a Metrohm Autolab PGSTAT204 electrochemical station in a typical three-electrode mode with 0.2 M Na_2SO_4 solution (pH = 6.8) as the electrolyte. A saturated Ag/AgCl electrode and a platinum (Pt) electrode were used as the reference electrode and counter electrode, respectively. A UV light with optical powder efficiency of 142 mW/cm^2 (Beijing Perfectlight Co. Ltd) was used as light source.

2.5. Photocatalytic activity test

To investigate the photocatalytic Cr(VI) reduction performance of **BUC-20**, 200.0 mL potassium dichromate ($K_2Cr_2O_7$) aqueous with initial concentration of 10 mg/L (based on Cr(VI)) was selected to conduct photocatalytic reaction at ambient condition in a quartz reactor containing the 15.0 mg **BUC-20** powder under UV light illumination (500 W Hg lamp, Beijing Aulight Co., Ltd). Before the photocatalysis reaction, the suspension was magnetically stirred in dark for 60.0 min to guarantee the adsorption-desorption equilibrium. During the reaction, 1.5 mL aliquots were extracted at 5.0 min time intervals using 0.45 μm syringe filter (Shanghai Troody) for analysis. The Cr (VI) residual concentration of samples were determined at 540 nm using diphenylcarbazide (DPC) method [2,36].

3. Results and discussion

3.1. Crystal structure analyses

The X-ray single-crystal diffraction data analysis (Table 1, Table 2 and Fig. 1) revealed that, in **BUC-20**, the octahedral geometry of the divalent Cu1 was completed by four oxygens occupying the four sites of the equatorial plane from two L ligands, and two nitrogen atoms at the two axial positions from two L ligands (Fig. 1a). As well, the monovalent Cu2 exhibited T-shaped geometry, which was

Table 1
Crystal structure data and refinement parameters for **BUC-20**.

Formula $C_{58}H_{56}Cu_3N_8O_{14}$	μ(Mo, Kα) (mm^{-1}) 1.205
M 1279.73	Total Reflections 6841
Crystal system Triclinic space group P$\bar{1}$	Unique 794
a, (Å) 10.7340 (9)	F (000) 659
b, (Å) 10.8621 (9)	Goodness-of-fit on F^2 1.049
c, (Å) 12.4909 (11)	R_{int} 0.044
α, (°) 88.993 (2)	R_1 0.0732
β, (°) 73.900 (1)	ωR_2 0.1961
γ, (°) 88.122 (2)	R_1 (all data) 0.1344
V, ($Å^3$) 1398.4 (2)	ωR_2 (all data) 0.2324
Z 1	Largest diff. Peak and hole (e/$Å^3$) 1.751,-0.992

Table 2
Selected bond lengths (Å) and angles (°) for **BUC-20**.

Bond lengths (Å)			
Cu(1)-O (3)#1	1.937 (4)	Cu(1)-O (1)	1.947 (4)
Cu(1)-O (3)	1.937 (4)	Cu(2)-N (4)#2	1.898 (5)
Cu(1)-O (1)#1	1.947 (4)	Cu(2)-N (3)	1.904 (5)
Bond angles (°)			
O (3)#1-Cu(1)-O (3)	180	C (5)-N (2)-C (13)	115.0 (6)
O (3)#1-Cu(1)-O (1)#1	90.94 (17)	C (3)-N (2)-C (13)	117.3 (5)
O (3)-Cu(1)-O (1)#1	89.06 (17)	C (24)-N (3)-C (20)	117.4 (5)
O (3)#1-Cu(1)-O (1)	89.06 (17)	C (24)-N (3)-Cu(2)	122.4 (5)
O (3)-Cu(1)-O (1)	90.94 (17)	C (20)-N (3)-Cu(2)	120.2 (5)
O (1)#1-Cu(1)-O (1)	180.000 (1)	C (29)-N (4)-C (25)	117.0 (5)
N (4)#2-Cu(2)-N (3)	173.2 (3)	C (29)-N (4)-Cu(2)#3	120.7 (5)
C (5)-N (1)-C (2)	112.5 (5)	C (25)-N (4)-Cu(2)#3	122.1 (4)
C (5)-N (1)-C (6)	123.1 (7)	C (1)-O (1)-Cu(1)	131.5 (4)
C (2)-N (1)-C (6)	124.4 (6)	C (4)-O (3)-Cu(1)	120.5 (4)
C (5)-N (2)-C (3)	108.4 (5)		

Symmetry transformations used to generate equivalent atoms: #1 -x+1,-y+2,-z; #2 x,y+1,z; #3 x,y-1,z

constructed from two nitrogen atoms from two different bpy ligands, and one oxygen atom from the L ligand (Fig. 1a). The O1, O3 and N2 from one L ligand were coordinated to Cu1 center, and the O3 atom was also joined to Cu2 center, which was quite different from the coordination modes in previously reported ones [34,44]. The co-existence Cu^{I} and Cu^{II} in **BUC-20** was affirmed by X-Ray photoelectron spectroscopy (XPS). As illustrated in Fig. 2a, the XPS peaks of 932.77 eV and 952.77 eV could be assigned to the 2p3/2 and 2p1/2 of Cu^{I}, and the satellite peaks at 942.22 eV and 962.62 eV implied the presence of Cu^{II} in BUC-20 coordination polymer [49]. As illustrated in Fig. 2b, the divalent Cu1 is coordinated by two completely deprotonated L^{2-} into discrete anionic $[CuL]^{2-}$ unit, and the monovalent Cu2 atoms are joined by bidentate bpy into 1D infinite $[Cu(bpy)]_n^{n+}$ chain. The adjacent $[Cu(bpy)]_n^{n+}$ chains are linked by oxygen atoms from L^{2-} ligands into double chain, in which the discrete $[CuL]^{2-}$ anions are embedded. The lattice water molecules are situated among the double chains, and are further stabilized by abundant hydrogen bonding interactions (Fig. 1c and Table 3).

3.2. Characterizations

BUC-20 was stable under air, as well stable/insoluble in water and common solvents like acid liquor (pH = 2.0), alkali liquor (pH = 8.0), ethanol, methylbenzene, chloroform, ether, dimethyl sulfoxide (DMSO) and N,*N*-dimethyl formamide (DMF), as illustrated in Fig. 2c. The TGA results revealed that the four lattice water molecules are lost until 201 °C with 5.63% weight loss (calculated value being 5.67%), and the framework of **BUC-20** is maintained well before 350 °C (Fig. 2e). The UV—vis diffuse reflectance spectroscopy (DRS) revealed that **BUC-20** has a strong absorption in the UV region, and the band gap (E_g) was estimated at 3.24 using the Kubelka-Munk function as shown Fig. 2b, implying that it has potential applications in photocatalytic reactions under UV light irradiation [34,35,44].

The transient photocurrent responses measurements were generally carried out to determine the charge-separation efficiency of photocatalyst [2,33,36,37]. As demonstrated in Fig. 2f, the strong photocurrent response was presented under the illumination of UV light, and the photocurrent rapidly decreased as the light was turned off. The photocurrent results indicated that **BUC-20** can be photoexcited to produce electron-hole pairs, which can be further separated rapidly. In addition, the results of Mott-Schottky measurements, illustrated Fig. 2e, revealed that the flat band potentials (E_{CB}) of **BUC-20** is −1.48 eV vs Ag/AgCl at pH = 6.8 according to positive slope of C^2 values versus potential. The Cr(VI)/Cr(III)

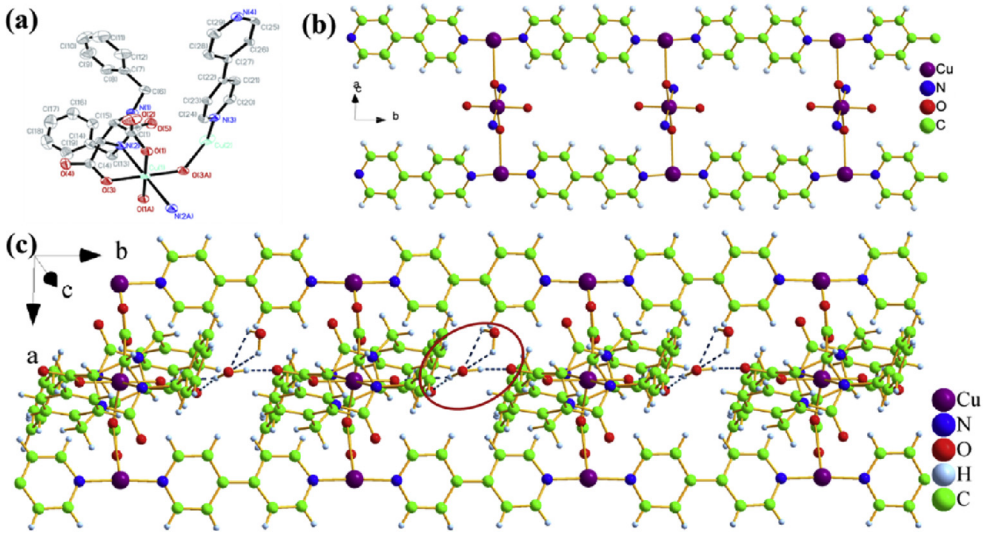

Fig. 1. (a) Coordination environment of Cu^{II} and Cu^{I} in $[Cu^{II}(L)_2][Cu^{I}(bpy)]_2 \cdot 4H_2O$ (**BUC-20**). Lattice water molecules and H atoms are omitted for clarity. (b) The simplified 1D infinite chain of **BUC-20**, in which the coordination environments of $Cu1^{II}$ and $Cu2^{I}$ were highlighted. (c) The 1D infinite chain of **BUC-20**.

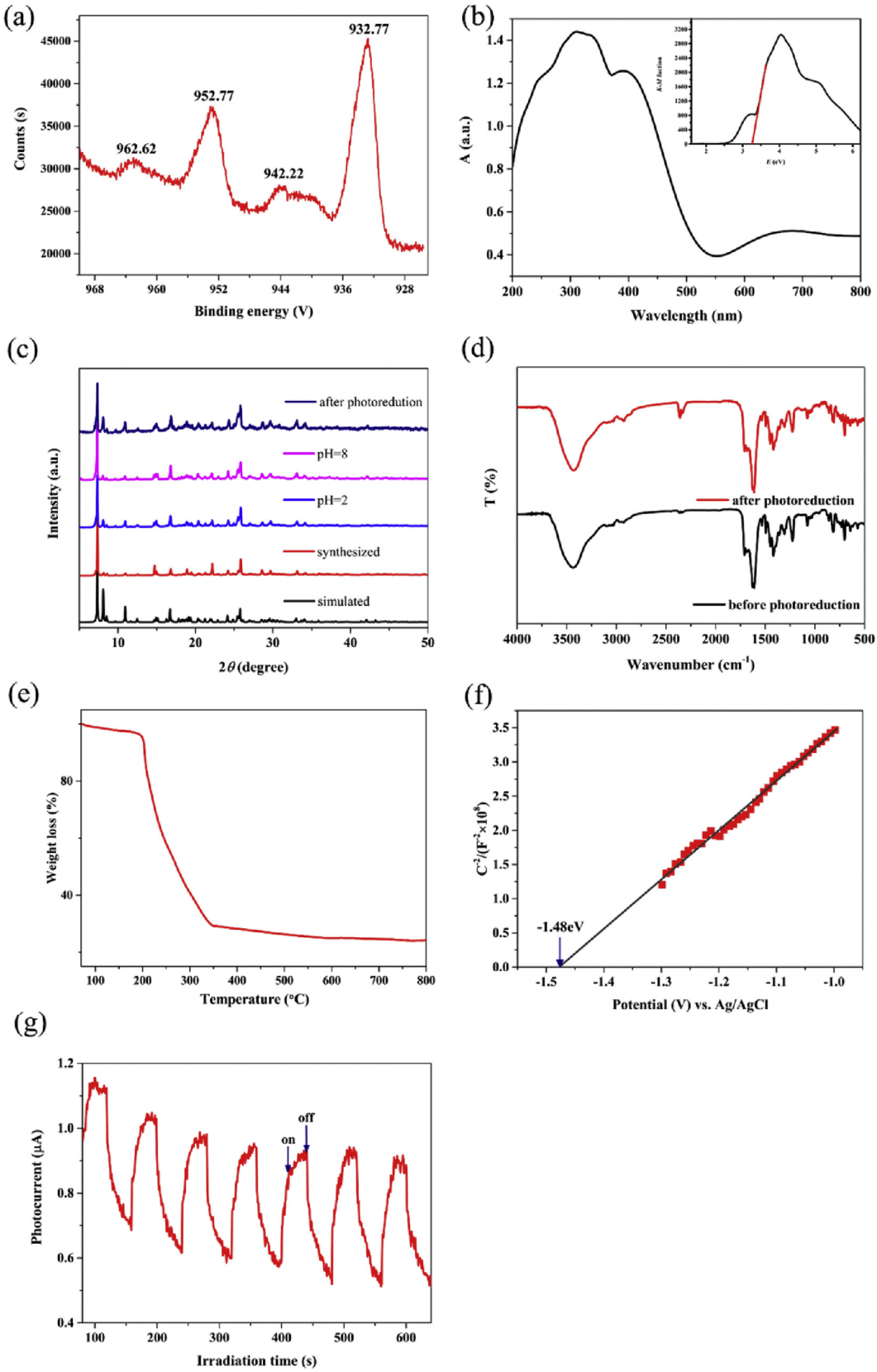

Fig. 2. (a) The XPS spectrum of Cu2p in **BUC-20**. (b) The UV–vis spectrum of **BUC-20**, and the insert shows Kubelka-Munk-transformed diffuse reflectance spectrum of **BUC-20**. (c) The PXRD patterns of **BUC-20** under different conditions. (d) The FTIR spectra before and after photoreduction upon **BUC-20**. (e) The TGA plot of **BUC-20**. (f) Mott-Schottky curve of **BUC-20** at frequencies of 500 Hz. (g) The transient photocurrent response of **BUC-20** in 0.2 M Na_2SO_4 aqueous solution under UV light irradiation.

Table 3
Hydrogen bonds for **BUC-20** [Å and °].

D-H	d (D-H)	d (H..A)	<DHA	d (D..A)	A
O6-H6E	0.85	1.827	162.39	2.649	O2
O6-H6F	0.85	2.169	163.34	2.993	O2 [-x+1,-y+1,-z]
O6-H6F	0.85	2.491	140.22	3.191	O1 [-x+1,-y+1,-z]
O7-H7C	0.85	2.18	112.09	2.621	O6
O7-H7D	0.85	2.166	113.27	2.621	O6

potentials under pH = 6.8 and 2.0 are calculated as +0.38 eV and +1.05 eV, respectively, based on $E = E^{o}$-0.14 pH derived from Nernst equation ($E^{o} = 1.33$ eV under the conditions of $T = 298$ K and pH = 0). The E_{CB} (−1.48 eV) of **BUC-20** was more negative than the Cr(VI)/Cr(III) potential under reaction conditions of $T = 298$ K and pH = 2.0, indicating the photo-induced electrons can be moved to reduce Cr(VI) into Cr(III).

3.3. Photocatalytic Cr(VI) reduction activity

The photocatalytic experiments revealed that **BUC-20** can accomplish nearly 100% Cr(VI) reduction under UV light irradiation and pH = 2.0 within 20.0 min, with the rate constant *K* being 0.1869 (Fig. 3a). For comparison, the ligand H_2L, commercial P25, **BUC-21** and **BUC-67** were adopted as photocatalysts under the identical conditions. The results displayed that within 30.0 min, ca. 20% and 80% Cr(VI) were reduced into Cr(III) in the presence of P25 and H_2L as photocatalysts, respectively, while almost 100% Cr(VI) was transformed into Cr(III) with the help of **BUC-21** (the rate constant *K* being 0.1069) or **BUC-67** (the rate constant *K* being 0.1100). It was concluded that the photocatalytic performance of **BUC-20** under UV light irradiation was superior to that of P25, **BUC-21**, **BUC-66** and **BUC-67**. Also, as listed in Table 4, the Cr(VI) reduction efficiency over **BUC-20** was better than that of TiO_2 and 3.0%Nd-TiO_2 reported

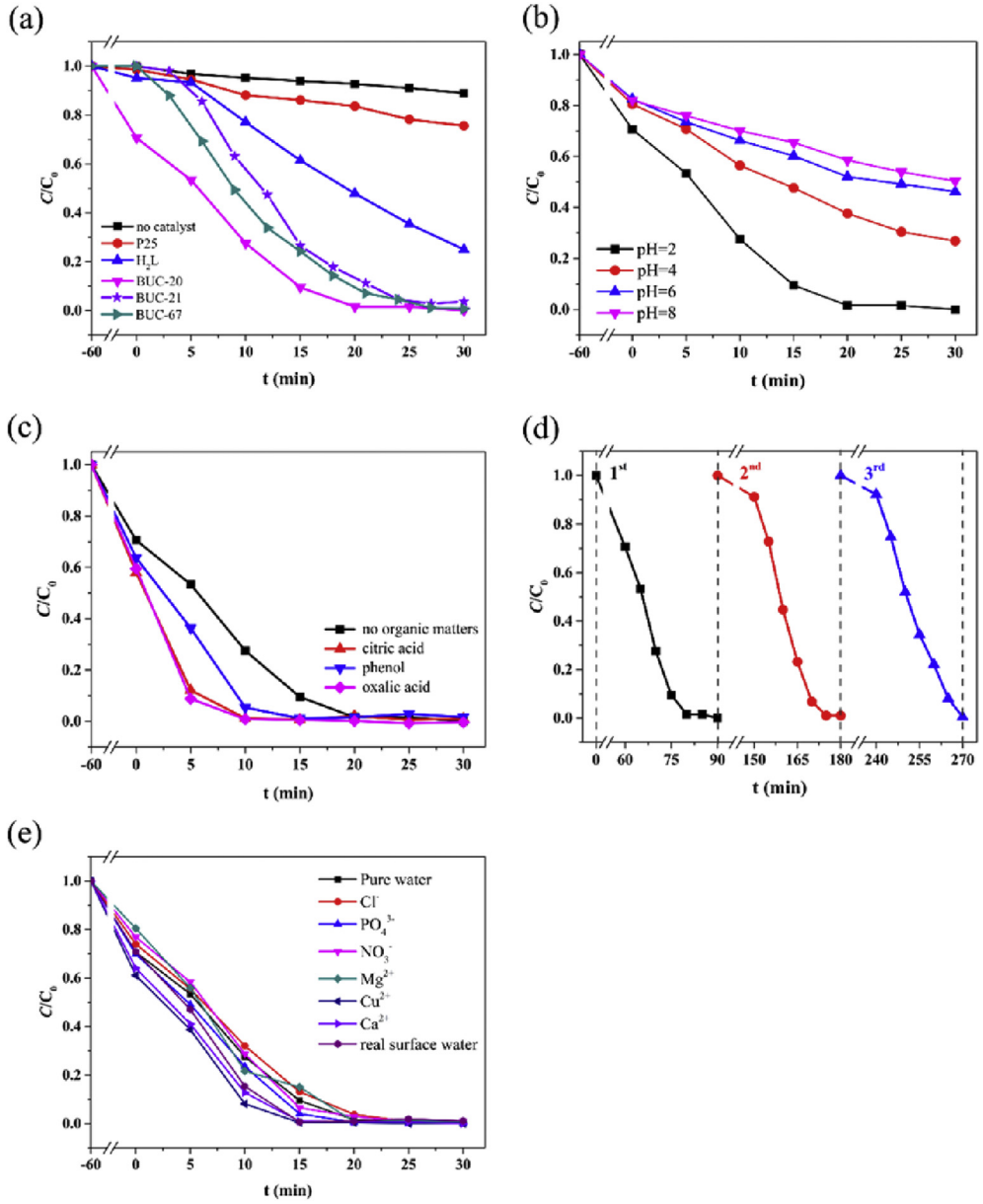

Fig. 3. (a) The Cr(VI) reduction efficiencies over different photocatalysts under identical conditions; (b) The Cr(VI) reduction efficiencies over **BUC-20** under different pH conditions; (c) The Cr(VI) reduction efficiencies over **BUC-20** with the presence of different organic matters; (d) Reusability of **BUC-20** as photocatalyst to conduct Cr(VI) reduction for 3 successive cycles. (e) The Cr(VI) reduction efficiencies over **BUC-20** with the presence of different foreign inorganic ions (1 mmol/L) and the simulated wastewater prepared with real surface water.

Table 4
Performance of some typical coordination polymers (including metal-organic frameworks) as photocatalysts for the Cr(VI) reduction under UV light irradiation.

Photocatalyst/Dosage (mg)	Cr(VI) solution Volume (mL)/concentration (ppm)/pH	hole scavenger	Time/ (min)	1st run cycle Reduction efficiency (%)	Times/last run cycle Reduction efficiency (%)	Ref.
TiO_2/1000	2200/10/3.0	ethanol	300	70	NA	[50]
3.0%Nd-TiO_2/250	250/10/3.1	NA	20	100	NA	[51]
P25	200/10/2.0	NA	30	40	NA	[34]
BUC-21/15	200/10/2.0	NA	30	96	3/94	[34]
BUC-66/15	200/10/2.0	NA	30	98	5/95	[44]
BUC-67/15	200/10/2.0	NA	30	99	5/95	[44]
BUC-20/15	200/10/2.0	NA	20	100	3/99	This work

previously [50,51]. The enhanced Cr(VI) removal efficiency of **BUC-20** could be contributed to the better adsorption activity toward Cr(VI) under dark condition resulted from its positive surface (+0.87 mV, pH = 2.0).

The pH values of the targeted solution not only exert significant influence on the existence form of Cr(VI), but also alter the surface characteristics of the photocatalysts to affect the reaction efficiency along with reaction rate. The photocatalytic Cr(VI) reduction performances under different pHs ranging from 2.0 to 8.0 were assessed under the identical conditions. The results illustrated in Fig. 3b revealed that with the increase of pH, the Cr(VI) reduction efficiencies and rates decreased significantly. (i) The H^+ was involved in the photocatalytic Cr(VI) reduction process (Equation (2)). Under acid condition, the abundant H^+ can facilitate the transformation from Cr(VI) to Cr(III). (ii) Under higher pH conditions, the formed Cr(III) can be easily precipitated into $Cr(OH)_3$ due to its low K_{sp} constant (Equation (3)), which might mask the active site of **BUC-20** photocatalyst to decline the photocatalytic activity. (iii) The zeta potential determination revealed that under the lower pH, the surface of **BUC-20** was more negative, which resulted into poorer adsorption performance toward Cr(VI) due to electric charges repel. As above-stated, acid condition like pH being 2.0 was optimal for the photocatalytic Cr(VI) reduction.

$$\textbf{BUC-20} + h\upsilon \rightarrow \textbf{BUC-20}\,(h^+ + e^-) \quad (1)$$

$$Cr_2O_7^{2-} + 14H^+ + 6e^- \rightarrow 2Cr^{3+} + 7H_2O \quad (2)$$

$$Cr^{3+} + 3OH^- \rightarrow Cr(OH)_3\downarrow \quad (3)$$

$$h^+ + 2H_2O + O_2 \rightarrow 2H_2O_2 \quad (4)$$

Considering the co-existence of organic pollutants and inorganic salts in real wastewater, it was necessary to investigate their influences toward photocatalytic Cr(VI) reduction. Three organic matters like phenol (0.2 mmol/L), oxalic acid (0.2 mmol/L) and citric acid (0.2 mmol/L) were selected as organic models. The results as illustrated in Fig. 3c revealed that the addition of these three organic compounds could significantly enhance the Cr(VI) reduction. Generally, during the photocatalytic Cr(VI) reduction process, the photo-induced electrons on LUMO (Lower Unoccupied Molecular Orbital) were consumed by Cr(VI), and the accumulated holes on HOMO (Highest Occupied Molecular Orbital) were reacted with water molecules to form H_2O_2 if there were no organic compounds in this system (Equation (4)). Once organic compounds were introduced into the system, the holes might be quickly consumed to accomplish quicker electron-hole separation, resulting into more efficient Cr(VI) reduction.

To investigate the influence of inorganic salt ions, the real surface water (K^+, 4.5 mg/L; Na^+, 35.6 mg/L; Ca^{2+}, 67.4 mg/L; Mg^{2+}, 32.1 mg/L; Cl^-, 32.0 mg/L; NO_3^-, 11.8 mg/L; SO_4^{2-}, 174.1 mg/L; PO_4^{3-}, 0.4 mg/L; COD_{Mn}, 11.6 mg/L) sampled from the Ming Lake in DaXing campus of BUCEA was used to prepare the targeted Cr(VI) solution. As displayed in Fig. 3e, the photocatalytic Cr(VI) reduction efficiency (99.9% within 15 min) wasn't inhibited by the dissolved foreign ions in surface water, which was assigned to the presence of organic compounds. It was implied that **BUC-20** could be used to conduct Cr(VI) reduction in real wastewater containing Cr(VI).

It is necessary to test the recyclability and stability of the photocatalyst for practical applications. As demonstrated in Fig. 3d, the Cr(VI) reduction efficiencies over **BUC-20** under the identical condition were 100%, 100% and 99% within 30 min for the first, second and third run, implying that **BUC-20** was highly stable and reusable. As well, the PXRD patterns and FTIR spectra of the used **BUC-20** matches well with the simulated ones from the single crystal data (Fig. 2c and d), implying **BUC-20** possessed good reusability and high stability toward Cr(VI) reduction.

Some previous studies displayed that Cr(VI) could be reduced into Cr(III) by the photo-catalytically induced electrons over coordination polymers (CPs) or metal-organic frameworks (MOFs), in which the corresponding mechanism was speculated [2,34–37,44]. To accomplish effective Cr(VI) reduction via photocatalysis, the bottom level of CB (conduction band) of photocatalyst had to be more negative than the Cr(VI)/Cr(III) redox potential [52]. The valance band edge potential (E_{VB}) was calculated as 1.76 eV from $E_{VB} = E_g + E_{CB}$, in which the conduction band edge potential (E_{CB}) and the band gap (E_g) are −1.48 eV (obtained from Mott-Schottky curve as illustrated in Fig. 2e) and 3.24 eV (based on calculated from DRS data as displayed in Fig. 2b), respectively. The E_{CB} of **BUC-20** is −1.48 V *vs* Ag/AgCl at pH = 6.8 (Fig. 2e), which is more negative than the Cr(VI)/Cr(III) potentials (+0.38 V, pH = 6.8; +1.05 V, pH = 2.0), implying that the photo-induced electrons in the CB of **BUC-20** can reduce Cr(VI) into Cr(III) [52].

4. Conclusion

A water-stable 1D coordination polymer **BUC-20** was successfully prepared under solvothermal condition, in which the co-existence of monovalent and divalent copper was further confirmed by XPS. **BUC-20** displayed excellent photocatalytic activity toward Cr(VI) reductions under UV light illumination and acid condition. The presence of organic matters can consume the accumulated holes in HOMO to facilitate the separation of photo-induced electron-hole pair, which resulted into the superior photocatalytic Cr(VI) reduction than existing photocatalysts under identical conditions. As well, the foreign inorganic ions possessed no significant impact on its photocatalytic performance, which was affirmed with the wastewater simulated with real surface water. **BUC-20** can be used for several runs due to good water stability. To utilize the visible light or even real sunlight, some visible light responsive semiconductor photocatalysts like g-C_3N_4, $Cd_{0.5}Zn_{0.5}S$ can be introduced to construct heterojunctions, which was affirmed as feasible strategy to accomplish the enhanced

photocatalytic activity under visible light.

Acknowledges

This work was supported by the National Natural Science Foundation of China (51578034, 51878023), Great Wall Scholars Training Program Project of Beijing Municipality Universities (CIT&TCD20180323), the Project of Construction of Innovation Teams and Teacher Career Development for Universities and Colleges Under Beijing Municipality (IDHT20170508), the Beijing Talent Project (2018A35).

Supplementary materials

CCDC 1882018 contains the supplementary crystallographic data for **BUC-20**. The data can be obtained free of charge from the Cambridge Crystallographic Data Centre via www.ccdc.cam.ac.uk/data_request/cif, or from the Cambridge Crystallographic Data Centre, 12 Union Road, Cambridge CB2 1EZ, UK; fax: (+44) 1223-336-033; or e-mail: deposit@ccdc.cam.ac.uk.

References

[1] F. Zhang, Y. Zhang, G. Zhang, Z. Yang, D.D. Dionysiou, A. Zhu, Appl. Catal. B Environ. 236 (2018) 53–63.
[2] C.-C. Wang, X.-D. Du, J. Li, X.-X. Guo, P. Wang, J. Zhang, Appl. Catal. B Environ. 193 (2016) 198–216.
[3] C.-C. Wang, Y.-S. Ho, Scientometrics 109 (2016) 481–513.
[4] J.-M. Hu, V.A. Blatov, B. Yu, K. Van Hecke, G.-H. Cui, Dalton Trans. 45 (2016) 2426–2429.
[5] X.-J. Kong, Y.-Z. Zhang, T. He, X.-Q. Wu, M.-M. Xu, S.-N. Wang, L.-H. Xie, J.-R. Li, CrystEngComm 20 (2018) 6018–6025.
[6] X. Wang, J. Sun, H. Lin, Z. Chang, X. Wang, G. Liu, Dalton Trans. 45 (2016) 12465–12478.
[7] C.A. Stackhouse, S. Ma, Polyhedron 145 (2018) 154–165.
[8] P. Li, B. Wang, Isr. J. Chem. 58 (2018) 1010–1018.
[9] B. Li, Y. Belmabkhout, Y. Zhang, P.M. Bhatt, H. He, D. Zhang, Y. Han, M. Eddaoudi, J.A. Perman, S. Ma, Chem. Commun. 52 (2016) 13897–13900.
[10] L. Li, R.-B. Lin, R. Krishna, H. Li, S. Xiang, H. Wu, J. Li, W. Zhou, B. Chen, Science 362 (2018) 443–446.
[11] A. Cadiau, K. Adil, P.M. Bhatt, Y. Belmabkhout, M. Eddaoudi, Science 353 (2016) 137–140.
[12] P.-Q. Liao, N.-Y. Huang, W.-X. Zhang, J.-P. Zhang, X.-M. Chen, Science 356 (2017) 1193–1196.
[13] H. Li, K. Wang, Y. Sun, C.T. Lollar, J. Li, H.-C. Zhou, Mater. Today 21 (2018) 108–121.
[14] S.E. Bambalaza, H.W. Langmi, R. Mokaya, N.M. Musyoka, J. Ren, L.E. Khotseng, J. Mater. Chem. 6 (2018) 23569–23577.
[15] X. Wu, L. Peng, S. Xiang, W. Cai, Phys. Chem. Chem. Phys. 20 (2018) 30150–30158.
[16] J. Camp, V. Stavila, M.D. Allendorf, D. Prendergast, M. Haranczyk, J. Phys. Chem. C 122 (2018) 18957–18967.
[17] C.A. Trickett, T.M. Osborn Popp, J. Su, C. Yan, J. Weisberg, A. Huq, P. Urban, J. Jiang, M.J. Kalmutzki, Q. Liu, J. Baek, M.P. Head-Gordon, G.A. Somorjai, J.A. Reimer, O.M. Yaghi, Nat. Chem. (2018), https://doi.org/10.1038/s41557-018-0171-z.
[18] I. Luz, F.X. Llabrés i Xamena, A. Corma, J. Catal. 276 (2010) 134–140.
[19] J. Lee, O.K. Farha, J. Roberts, K.A. Scheidt, S.T. Nguyen, J.T. Hupp, Chem. Soc. Rev. 38 (2009) 1450–1459.
[20] F. Gándara, A.d. Andrés, B. Gómez-Lor, E. Gutiérrez-Puebla, M. Iglesias, M.A. Monge, D.M. Proserpio, N. Snejko, Cryst. Growth Des. 8 (2008) 378–380.
[21] P. Mahata, S.K. Mondal, D.K. Singha, P. Majee, Dalton Trans. 46 (2017) 301–328.
[22] H. Li, Y. Han, Z. Shao, N. Li, C. Huang, H. Hou, Dalton Trans. 46 (2017) 12201–12208.
[23] X.-X. Song, H. Fu, P. Wang, H.-Y. Li, Y.-Q. Zhang, C.-C. Wang, J. Colloid Interface Sci. 532 (2018) 598–604.
[24] A. Liu, C.-Z. Wang, C. Chu, H.-Y. Chu, X. Chen, A.-F. Du, J. Mao, W. Zheng, C.-C. Wang, J. Environ. Chem. Eng. 6 (2018) 4961–4969.
[25] X.-Y. Xu, C. Chu, H. Fu, X.-D. Du, P. Wang, W. Zheng, C.-C. Wang, Chem. Eng. J. 350 (2018) 436–444.
[26] A. Liu, C.-C. Wang, C.-z. Wang, H.-f. Fu, W. Peng, Y.-L. Cao, H.-Y. Chu, A.-F. Du, J. Colloid Interface Sci. 512 (2018) 730–739.
[27] X.-D. Du, C.-C. Wang, J.-G. Liu, X.-D. Zhao, J. Zhong, Y.-X. Li, J. Li, P. Wang, J. Colloid Interface Sci. 506 (2017) 437–441.
[28] J.-J. Li, C.-C. Wang, H.-f. Fu, J.-R. Cui, P. Xu, J. Guo, J.-R. Li, Dalton Trans. 46 (2017) 10197–10201.
[29] X.-D. Du, C.-C. Wang, J. Zhong, J.-G. Liu, Y.-X. Li, P. Wang, J. Environ. Chemi. Eng. 5 (2017) 1866–1873.
[30] Y. Li, Z. Yang, Y. Wang, Z. Bai, T. Zheng, X. Dai, S. Liu, D. Gui, W. Liu, M. Chen, L. Chen, J. Diwu, L. Zhu, R. Zhou, Z. Chai, T.E. Albrecht-Schmitt, S. Wang, Nat. Commun. 8 (2017) 1354.
[31] T. Zheng, Z. Yang, D. Gui, Z. Liu, X. Wang, X. Dai, S. Liu, L. Zhang, Y. Gao, L. Chen, D. Sheng, Y. Wang, J. Diwu, J. Wang, R. Zhou, Z. Chai, T.E. Albrecht-Schmitt, S. Wang, Nat. Commun. 8 (2017) 15369.
[32] L. Zhu, D. Sheng, C. Xu, X. Dai, M.A. Silver, J. Li, P. Li, Y. Wang, Y. Wang, L. Chen, C. Xiao, J. Chen, R. Zhou, C. Zhang, O.K. Farha, Z. Chai, T.E. Albrecht-Schmitt, S. Wang, J. Am. Chem. Soc. 139 (2017) 14873–14876.
[33] C.-C. Wang, J.-R. Li, X.-L. Lv, Y.-Q. Zhang, G. Guo, Energy Environ. Sci. 7 (2014) 2831–2867.
[34] F.-X. Wang, X.-H. Yi, C.-C. Wang, J.-G. Deng, Chin. J. Catal. 38 (2017) 2141–2149.
[35] X.-D. Du, X.-H. Yi, P. Wang, W. Zheng, J. Deng, C.-C. Wang, Chem. Eng. J. 356 (2019) 393–399.
[36] X. Du, X. Yi, P. Wang, J. Deng, C.-c. Wang, Chin. J. Catal. 40 (2019) 70–79.
[37] X.-H. Yi, F.-X. Wang, X.-D. Du, P. Wang, C.-C. Wang, Appl. Organomet. Chem. 33 (2019) e4621.
[38] C. Jiao, X. Jiang, H. Chu, H. Jiang, L. Sun, CrystEngComm 18 (2016) 8683–8687.
[39] D. Sadhukhan, C. Rizzoli, E. Garribba, C.J. Gómez-García, A. Yahia-Ammar, L.J. Charbonnière, S. Mitra, Dalton Trans. 41 (2012) 11565–11568.
[40] S.J. Ferrara, B. Wang, J.P. Donahue, Dalton Trans. 45 (2016) 2997–3002.
[41] X.-P. Zhou, D. Li, S.-L. Zheng, X. Zhang, T. Wu, Inorg. Chem. 45 (2006) 7119–7125.
[42] G. Givaja, P. Amo-Ochoa, C.J. Gómez-García, F. Zamora, Chem. Soc. Rev. 41 (2012) 115–147.
[43] Y. Li, H. Xu, S. Ouyang, J. Ye, Phys. Chem. Chem. Phys. 18 (2016) 7563–7572.
[44] X.-H. Yi, F.-X. Wang, X.-D. Du, H. Fu, C.-C. Wang, Polyhedron 152 (2018) 216–224.
[45] Bruker AXS, SMART, Version 5.611, Bruker AXS, Madison, WI, USA, 2000.
[46] Bruker AXS, SAINT, Version 6.28, Bruker AXS, Madison, WI, USA, 2003.
[47] SADABS, V2.03, Bruker AXS, Madison, WI, 2000.
[48] G.M. Sheldrick, SHELX-97, GÖttingen University, Germany, 1997.
[49] Y. Zhu, W.-y. Wang, M.-w. Guo, G. Li, H.-j. Lu, Inorg. Chem. Commun. 14 (2011) 1432–1435.
[50] Y. Ku, I.-L. Jung, Water Res. 35 (2001) 135–142.
[51] S. Rengaraj, S. Venkataraj, J.-W. Yeon, Y. Kim, X.Z. Li, G.K.H. Pang, Appl. Catal. B Environ. 77 (2007) 157–165.
[52] L. Wang, X. Li, W. Teng, Q. Zhao, Y. Shi, R. Yue, Y. Chen, J. Hazard Mater. 244–245 (2013) 681–688.